*Modern Chemistry*
2024, Vol. 12, No. 3, pp. 47-59
https://doi.org/10.11648/j.mc.20241203.11

Research Article

# Synthesis and Characterization of Highly Efficient Cu-BTC MOF, ($[Cu_3(C_9H_3O_6)_2]._3H_2O\{18H_2O\}$) Photocatalyst for the Adsorptive Transformation of Coloured Organic Pollutants in Water

**Aba Akebi Atta-Eyison[1], Ruphino Zugle[2, *]**

[1]Industrial and Health Sciences Department, Takoradi Technical University, Takoradi, Ghana
[2]Department of Chemistry, University of Cape Coast, Cape Coast, Ghana

## Abstract

Photocatalysis has garnered significant attention for its potential in environmental remediation, energy conversion, and sustainable chemistry. Metal-organic frameworks (MOFs) have emerged as promising photocatalytic materials due to their tunable structures, high surface areas, and unique optical properties. Among them, a newly synthesized copper-benzene-1, 3, 5-tricarboxylic acid (Cu-BTC) MOF, $[Cu_3(C_9H_3O_6)_2]._3H_2O\{18H_2O\}$ has shown remarkable potential as a photocatalyst. In this work, the synthesis and characterization of a novel $[Cu_3(C_9H_3O_6)_2]._3H_2O\{18H_2O\}$ for its photocatalytic applications is described. The synthesis of $[Cu_3(C_9H_3O_6)_2]._3H_2O\{18H_2O\}$ was achieved through a solvothermal method employing Copper (II) Nitrate trihydrate and benzene-1, 3, 5-tricarboxylic acid as precursors in a suitable solvent. The synthesized $[Cu_3(C_9H_3O_6)_2]._3H_2O\{18H_2O\}$) was characterized by Fourier transform infrared (FTIR), X-ray diffraction (XRD), Scanning electron microscope-energy dispersive X-ray spectroscopy (SEM-EDS), Single crystal and Thermogravimetric (TGA) analysis. The photocatalytic activity of ($[Cu_3(C_9H_3O_6)_2]._3H_2O\{18H_2O\}$) was evaluated in the transformation of Lissamine green SF (LGSF) and Tetraethylrhodamine (TeRh) under solar light irradiation. The intermediate compounds obtained during the transformation of LGSF under photocatalysis were detected using a gas chromatography-mass spectrometer (GC-MS). The recyclability of $[Cu_3(C_9H_3O_6)_2]._3H_2O\{18H_2O\}$was investigated to demonstrate its stability, robustness and potential for practical applications. Conclusively, the $[Cu_3(C_9H_3O_6)_2]._3H_2O\{18H_2O\}$ was proven to be an effective catalyst in the mineralization of LGSF and TeRh.

## Keywords

Metal-organic Frameworks, Solvothermal Synthesis, Characterization, Adsorption, Light Irradiation

## 1. Introduction

Copper (Cu) is one of the prevailing transition metal elements used as a metal centre for metal-organic frameworks (MOFs). Copper is abundant, less expensive, non-toxic and has amazing complexation strength [3, 4]. Copper-based

*Corresponding author: rzugle@ucc.edu.gh (Ruphino Zugle)

**Received:** 30 July 2024; **Accepted:** 26 August 2024; **Published:** 11 September 2024

MOFs are, therefore, easy to synthesize due to the remarkable complexation property of copper [5, 6]. The $d^9$ system of Cu (II) complexes leads to diversified structural geometries. Geometries such as square planar, tetrahedral, octahedral, trigonal planar, square pyramidal and trigonal bipyramid have been found [7-12]. Copper is one of the first transition elements to be used with benzene-1, 3, 5- tricarboxylic acid to synthesize HKUST-1 ($[Cu_3(BTC)_2 3H_2O]n$), which has served as a standard for adsorption studies for many years [13, 14]. After the discovery of the promising adsorption property of HKUST-1, numerous research into the synthesis of copper-base MOFs using different synthetic techniques including hydrothermal, solvothermal, microwave, and sonochemical techniques with varying parameters have been investigated for different applications with a recent focus on photocatalysis [15-21].

Copper-base MOFs as photocatalysts should have the ability to capture light and have a light excitation period that produces charge separation. An efficient electron-hole separation is obtained in MOFs by the transfer of photogenerated electrons from the organic ligands onto the surfaces of metal clusters through ligand-to-metal charge transfer (LMCT) [22-25]. The amount of energy absorbed by MOF for excitation ($E_{abs}$) is directly related to the band gap ($E_g$) between the highest occupied molecular orbital (HOMO) and lowest unoccupied molecular orbital (LUMO) of ligands and the energy necessary to transfer the photogenerated electrons from the LUMO of the ligands to the LUMO of the metal clusters ($E_{LMCT}$) [22, 24, 26-28]. Charge separation is better when Eg is constant with $E_{LMCT}$ approaching zero or negative. This condition results in a smaller absorbed excitation energy (Eabs) to enhance visible light absorption. [29-32].

In a photocatalytic mineralization process, the HOMO/LUMO in MOFs performs a similar function as the conduction and valence band (CB/VB) in semiconductors [33-36]. During photocatalysis, ligand-to-metal charge transfer (LMCT) occurs. Electrons then transit from the highest occupied molecular orbital (HOMO) to the lowest unoccupied molecular orbital (LUMO) [37-40] of the metal. The transition of electrons from the HOMO leaves holes in the HOMO. The transitioned election in the LUMO is trapped by oxygen molecules reducing it to yield superoxide radical ($•O_2^-$). This radical is a strong oxidant which can react rapidly with adsorbed pollutants. The strong oxidative ability of the holes ($h^+$) generated in the HOMO enables the direct adsorption of pollutants and the oxidation of the surface hydroxyl group or water to generate hydroxyl radicals (•OH). The hydroxyl radicals (•OH) formed are also a strong oxidant which is capable of reacting eagerly with surface-adsorbed pollutants. The activity of these generated radicals and holes can lead to pollutant mineralization [41-44].

Recently, the use of Cu-BTC MOFs as photocatalysts for the mineralization of pollutants in water has been keenly investigated [45-55]. A comprehensive analysis has been conducted to highlight the wide range of advantageous characteristics exhibited by Cu-BTC MOF, establishing it as a highly versatile material with applications across various domains. Emphasis has been placed on its reactivity, the significance of the metal ion, and its recent potential in effectively tackling the removal of hazardous textile dye pollutants from wastewater effluent. Drawbacks such as low stability and low turnout in photocatalytic performance have, however, been observed. The photocatalytic performance of Cu-BTC is usually enhanced by hydrogen peroxide activity to generate sufficient radicals for the photocatalytic mineralization process [45, 46]. Additionally, most studies into the use of Cu-BTC MOFs as photocatalysts involve the modification of Cu-BTC MOFs into composites through post-synthesis to improve their stability and photocatalytic performance [47-55]. The low stability and low turnout in the photocatalytic performance of Cu-BTC MOFs may highly relate to inappropriate synthetic processes. The choice of reaction conditions, the duration and kinetics of the synthesis process as well as the ratio of metal ions to organic ligands during synthesis is critical. It is, therefore, vital to optimize the synthetic processes for Cu-BTC MOFs. As a result of this emerging exploitation, research into the synthesis of a highly effective stable copper MOF photocatalyst using the solvothermal synthetic technique to transform organic dyes into less toxic compounds in water was intended.

## 2. Materials and Methods

### 2.1. Materials

Copper (II) nitrate trihydrate (98-103%, Sigma Aldrich), Benzene- 1, 3, 5- tricarboxylic acid ($H_3BTC$) (95%, Aldrich Chemistry), Ultrapure water (100%,), methanol (99.9%, Daejung Chemicals and Metals Co. LTD), ethanol (99.6% J. T. Baker), Lissamine green SF (65%, Paskem Finechemical Industries) and Tetraethylrhodamine (≥95%, Paskem Finechemical Industries). The chemicals were used as obtained.

### 2.2. Synthesis of $[Cu_3(C_9H_3O_6)_2]._3H_2O\{18H_2O\}$

The synthesis of the Cu-BTC MOF, ($[Cu_3(C_9H_3O_6)_2]._3H_2O\{18H_2O\}$), was a modification of the synthetic procedure reported in previous works [57, 58]. A 60 mL solution (15 mL ethanol /45 mL ultrapure water) containing 3.5 mmol 1, 3, 5-benzene tricarboxylic acid (($H_3BTC$) and 5 mmol of Copper (II) Nitrate trihydrate was heated at 120 ℃ for 18 hours in Teflon liner autoclave. The acquired compound was filtered, washed thoroughly with methanol and dried in the oven at 70 ℃ overnight to acquire a blue crystal product.

### 2.3. Characterization

Various test were done to characterize $H_3BTC$ and

$[Cu_3(C_9H_3O_6)_2].{}_3H_2O\{18H_2O\}$. Functional groups were identified by Fourier transform infrared (FTIR) analysis using the Bruker Alpha Spectrometer. The crystallinity was investigated using an Empyrean X-ray Diffractometer. The surface morphology and elemental analysis were analyzed using ZEISS EVO MA 15 SEM-EDS. The topology of $[Cu_3(C_9H_3O_6)_2].{}_3H_2O\{18H_2O\}$ through Single Crystal analysis was done using Rigaku 007VHF diffractometer. The thermal stability of the $[Cu_3(C_9H_3O_6)_2].{}_3H_2O\{18H_2O\}$ was examined using the SDT Q600 V20.9 System under a nitrogen atmosphere. The data for the various characterizations have been referenced [1]. A band gap analysis was performed by measuring the UV-visible absorption of $[Cu_3(C_9H_3O_6)_2].{}_3H_2O\{18H_2O\}$ using the T70 UV/VIS Spectrometer by PG Instruments Ltd.

### 2.4. Photo-Transformation Test

The photocatalytic activity of the synthesized $[Cu_3(C_9H_3O_6)_2].{}_3H_2O\{18H_2O\}$ was studied on Lissamine green SF (LGSF) and Tetraethylrhodamine (TeRh). For each photocatalytic activity, a 150 mL beaker containing 100 mL of sample pollutant solution and $[Cu_3(C_9H_3O_6)_2].{}_3H_2O\{18H_2O\}$ as catalyst was stirred in the dark for an hour to achieve adsorption/desorption equilibrium and then under solar light for 180 min. During the photocatalytic activity, a 5 mL aliquot was drawn at 30 min intervals to observe the absorbance.

### 2.5. Adsorption Study

The quantities of pollutants adsorbed on the surfaces of $[Cu_3(C_9H_3O_6)_2].{}_3H_2O\{18H_2O\}$ at a given time t, and at equilibrium, are obtained using equation (1) and equation (2).

$$q_t = \frac{(C_i - C_t)}{m} \times V \quad (1)$$

$$q_e = \frac{(C_i - C_e)}{m} \times V \quad (2)$$

Where; $q_t$(mg/g) is the adsorption capacity of $[Cu_3(C_9H_3O_6)_2].{}_3H_2O\{18H_2O\}$ at a given time, $q_e$(mg/g) is the adsorption capacity of $[Cu_3(C_9H_3O_6)_2].{}_3H_2O\{18H_2O\}$ at equilibrium, $C_i$ (mg/L) = initial concentration of pollutant in solution, $C_t$(mg/L) = concentration of pollutant in solution at time t, $C_e$ (mg/L) = concentration of pollutant in solution at equilibrium, V is the volume of solution (L) and m is the mass (g) of $[Cu_3(C_9H_3O_6)_2].{}_3H_2O\{18H_2O\}$. The pollutant percentage removal efficiency was calculated using Equation (3)

$$\text{Pollutant removal efficiency (\%)} = \frac{C_i - C_t}{C_i} \times 100\ \% \quad (3)$$

### 2.6. Transformed Compound Determination Test

SHIMADZA GC-MS QP 2020 was used to identify intermediate compounds from the transformed pollutants [2]. For the gas chromatogram (GC), a DB-5ms column of 30 m × 0.25 mm, 0.25 µm film thickness was employed. An injection pot temperature of 250 ℃ and splitless injection mode were employed with helium as the carrier gas. For the mass spectrometer (MS), the ion source temperature was 210 ℃. It was run on scan mode with start m/z 50.00 to m/z 1030.

## 3. Results

### 3.1. Characterization

To investigate the link between the metal and the ligand, Fourier transform infrared (FTIR) spectrum of $H_3BTC$ (a) and that of the $[Cu_3(C_9H_3O_6)_2].{}_3H_2O\{18H_2O\}$ (b) was investigated as shown in Figure 1. A shift of broadband to the left is observed for $[Cu_3(C_9H_3O_6)_2].{}_3H_2O\{18H_2O\}$ compared to that observed in $H_3BTC$. The broadband between 3650 $cm^{-1}$ to 2840 $cm^{-1}$ could be due to the presence of the OH group from water molecules adsorbed on the surface of the $[Cu_3(C_9H_3O_6)_2].{}_3H_2O\{18H_2O\}$ from its' hydrate salt [59-61]. The intense bands from 1370 $cm^{-1}$ to 1609 $cm^{-1}$ could be associated with the asymmetric and symmetric vibrational stretch of the carboxylate ($COO^-$) groups found in the $[Cu_3(C_9H_3O_6)_2].{}_3H_2O\{18H_2O\}$[61, 62]. The bands between 1100 $cm^{-1}$ to 680 $cm^{-1}$ relate to the in and out of plane vibrations of CH in the benzene ring found in $H_3BTC$ and $[Cu_3(C_9H_3O_6)_2].{}_3H_2O\{18H_2O\}$[60, 62, 63]. The bands at 660 $cm^{-1}$ and 480 $cm^{-1}$ in $[Cu_3(C_9H_3O_6)_2].{}_3H_2O\{18H_2O\}$ (b) could be a result of Cu–O bending and stretching vibrations similar to reports related to copper complexes [59, 64].

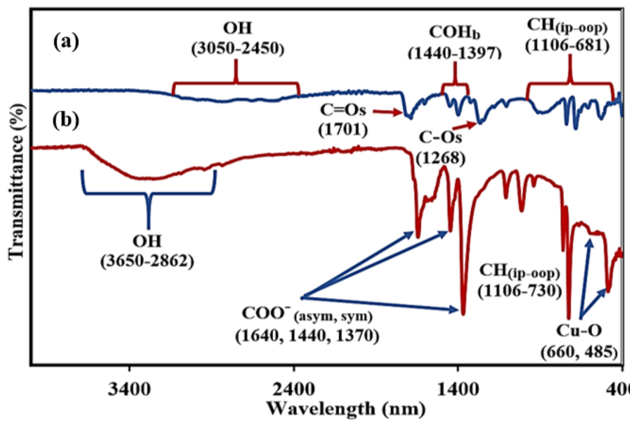


*Figure 1. FTIR of (a) $H_3BTC$ and (b) $[Cu_3(C_9H_3O_6)_2].{}_3H_2O\{18H_2O\}$.*

Crystallinity study of (a) $H_3BTC$ (a) and $[Cu_3(C_9H_3O_6)_2].{}_3H_2O\{18H_2O\}$ (b) through X-ray diffraction (XRD) analysis is shown in Figure 2 referenced in research data. The obtained XRD result of $[Cu_3(C_9H_3O_6)_2].{}_3H_2O\{18H_2O\}$ (b) indicates the formation of well-resolved peeks with main diffraction peaks at 6.70°, 9.48°, 11.62°, 13.43°, 16.50°, 17.48°, 19.05°, 20.21°, 24.16°, 25.97°, 29.35°, 35.50° and 39.28° which indicate a high degree of crystallinity. The diffraction peaks 6.70°, 9.48°, 11.62°, 13.43° and 29.35° were identifiable to similar angles for $H_3BTC$ (a).

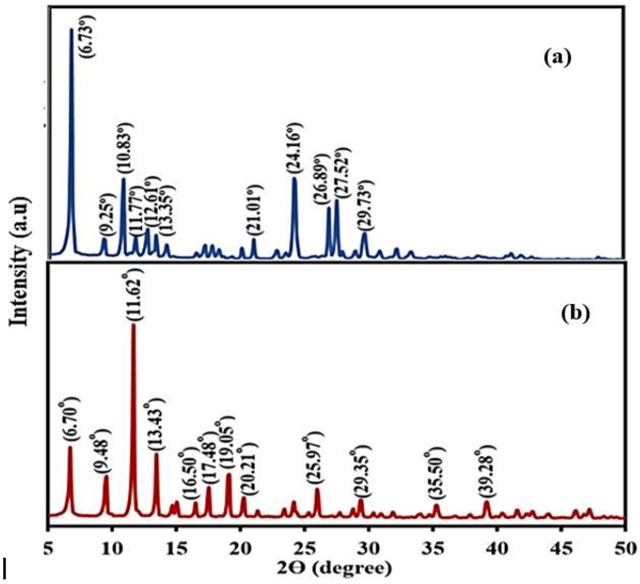


***Figure 2.*** *XRD of (a) $H_3BTC$ (b) ($[Cu_3(C_9H_3O_6)_2]._3H_2O\{18H_2O\}$).*

The morphology and elemental analysis of $H_3BTC$ (a) and $[Cu_3(C_9H_3O_6)_2]._3H_2O\{18H_2O\}$ (b) using scanning electron microscope-energy dispersive X-ray spectroscopy (SEM-EDS) is as shown in Figure 3. It is observed that $H_3BTC$ shows a close-packed arrangement with a cuboid-shaped morphology. The EDS spectrum revealed the presence of carbon (C) copper and oxygen (O) with atomic percentages of 64.62 % for carbon and 35.38 % for oxygen. SEM-EDS images of $[Cu_3(C_9H_3O_6)_2]._3H_2O\{18H_2O\}$ exhibited cubic crystal particles with trapezoid shapes. The EDS spectrum revealed the presence of carbon (C), copper (Cu) and oxygen (O) with atomic percentages of 58.22 % for carbon, 34.21 % for oxygen and 7.57% for copper (C).

Topology analysis of $[Cu_3(C_9H_3O_6)_2]._3H_2O\{18H_2O\}$ through Single crystal XRD is shown in Figure 4. The $[Cu_3(C_9H_3O_6)_2]._3H_2O\{18H_2O\}$ had a unit formula $C_6H1_6CuO_{11}$ and crystallizes in the Fm-3m space group with a grown view of each unit $[Cu_3(C_9H_3O_6)_2]._3H_2O\{18H_2O\}$ (a) consisting of an assembly of two linked copper atoms (Cu1) forming coordinates with four carboxylate oxygen atoms (O1) each and one oxygen atom (O2) each from coordinated $H_2O$ molecule [65, 66]. The unit assembly forms a cubic crystal system with a trapezoid shape having a size dimension of 0.10×0.09×0.07 $mm^3$ with a bond length of a = 26.2891(3) Å, b = 26.2891(3) Å, c = 26.2891(3) Å and bond angle, a = b = g = 90°. A water mask of V = 18168.8(6) Å3 was obtained for a void per unit cell. The coordination of the carboxylate oxygen, water oxygen and copper develops into a highly porous 3D network of metal-organic framework shown in Figure 4(b) having four pore centres.

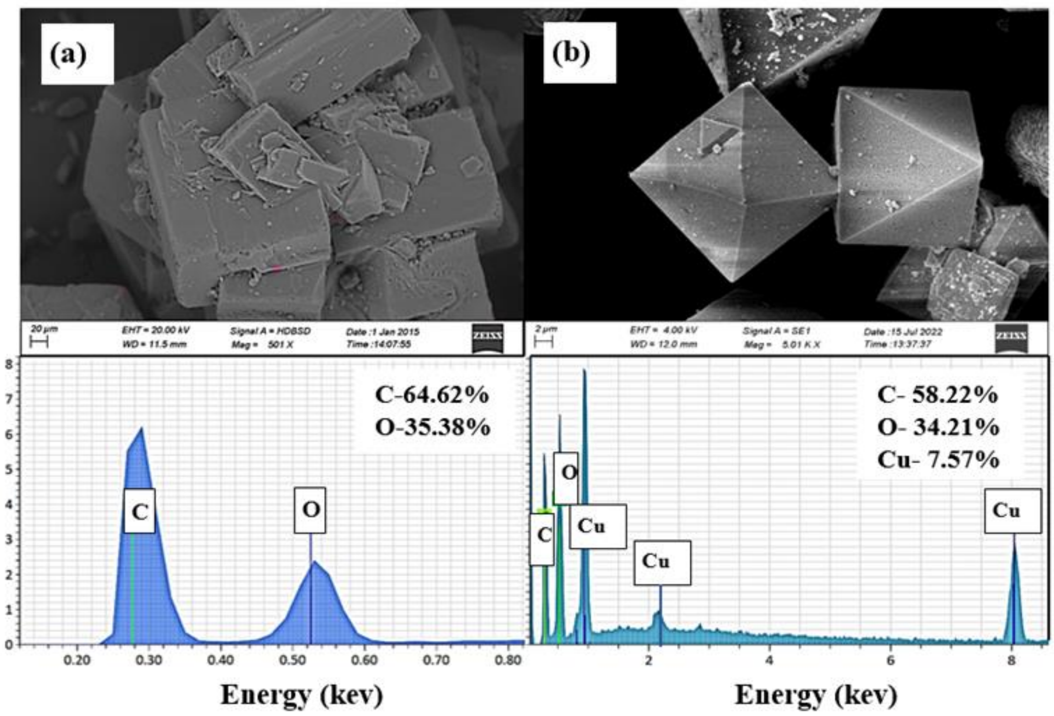


***Figure 3.*** *SEM-EDS of (a) $H_3BTC$ and (b) $[Cu_3(C_9H_3O_6)_2]._3H_2O\{18H_2O\}$.*

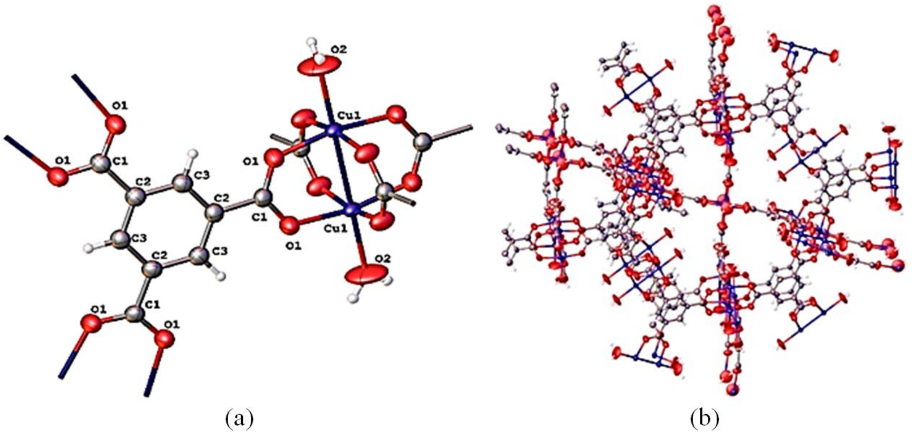


***Figure 4.*** *Single crystal XRD of (a) A grown view of* $[Cu_3(C_9H_3O_6)_2]._3H_2O\{18H_2O\}$ *(b) A 3D network of* $[Cu_3(C_9H_3O_6)_2]._3H_2O\{18H_2O\}$.

Thermogravimetric analysis (TGA) of $[Cu_3(C_9H_3O_6)_2]._3H_2O\{18H_2O\}$ is shown in Figure 5. Two main weight loss steps and corresponding rate of change of weight loss exothermic peaks were observed. The first weight loss percentage of 23.63% with a corresponding rate of change of weight loss of 7.31 %/min observed between 50 ℃ and 200 ℃ relates to the elimination of water molecules and organic solvents remaining in the $[Cu_3(C_9H_3O_6)_2]._3H_2O\{18H_2O\}$[58, 67]. A large percentage loss of 37.71% and a correspondingly high rate of change of weight loss of 22.64 %/min observed between 350 ℃ and 400 ℃ indicates the decomposition of $[Cu_3(C_9H_3O_6)_2]._3H_2O\{18H_2O\}$ due to the removal of ligand molecule from $[Cu_3(C_9H_3O_6)_2]._3H_2O\{18H_2O\}$[67, 68]. A slight decrease in the percentage weight loss observed in the range of 400–800 ℃ indicates the formation of copper oxide formed after the decomposition of the $[Cu_3(C_9H_3O_6)_2]._3H_2O\{18H_2O\}$[58, 59]. The decomposition of $[Cu_3(C_9H_3O_6)_2]._3H_2O\{18H_2O\}$ around 400 ℃ indicates it is thermally stable and will only disintegrate above 300 ℃.

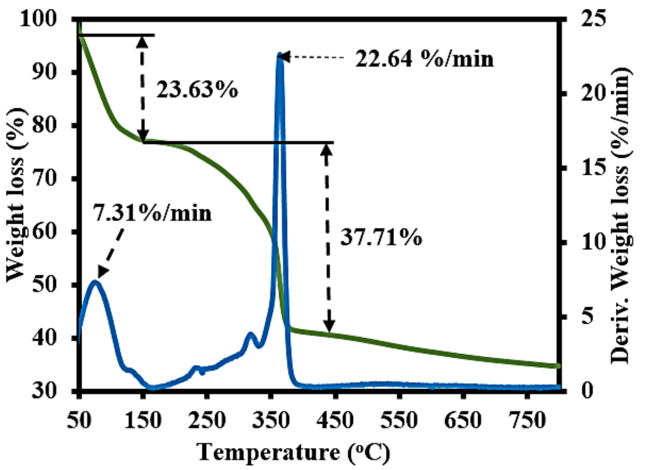


***Figure 5.*** *TGA-DSC of* $[Cu_3(C_9H_3O_6)_2]._3H_2O\{18H_2O\}$.

The UV-visible absorption spectrum of $[Cu_3(C_9H_3O_6)_2]._3H_2O\{18H_2O\}$ in Figure 6 shows a maximum absorption wavelength of 386 nm. The $E_g$ was subsequently calculated using Equation (4) [69, 70].

$$E_g = \frac{1240}{\lambda g} \tag{4}$$

Where, $E_g$ = band gap energy of photocatalyst in electron volt (eV) and $\lambda_g$ = absorption edge of photocatalyst in nanometers (nm). $E_g$ = 2.67 eV was observed. Schottky barrier height ($\Phi_B$) at equilibrium with graphical definition as the difference between the interfacial conduction band edge ($E_C$) and Fermi level ($E_F$) [71, 72] was recorded as 0.32ev.

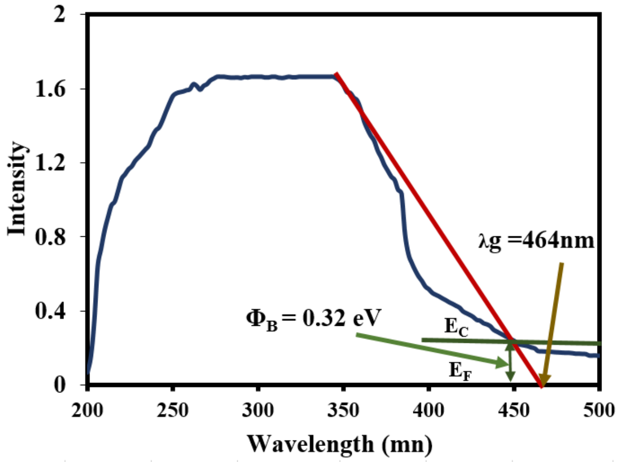


***Figure 6.*** *Uv-Visible absorption spectrum of* $[Cu_3(C_9H_3O_6)_2]._3H_2O\{18H_2O\}$.

## 3.2. Photo-Transformation Test

The photocatalytic ability of $[Cu_3(C_9H_3O_6)_2]._3H_2O\{18H_2O\}$ for the transformation of Lissamine green SF (LGSF) and Tetraethylrhodamine (TeRh) which resulted in their removal from water is shown in Figure 7. Over 80% pollutant removal was observed using $[Cu_3(C_9H_3O_6)_2]._3H_2O\{18H_2O\}$ as photocatalyst. The percentage of LGSF (92.56%) removal was however higher than that of TeRh (85.43%) removal.

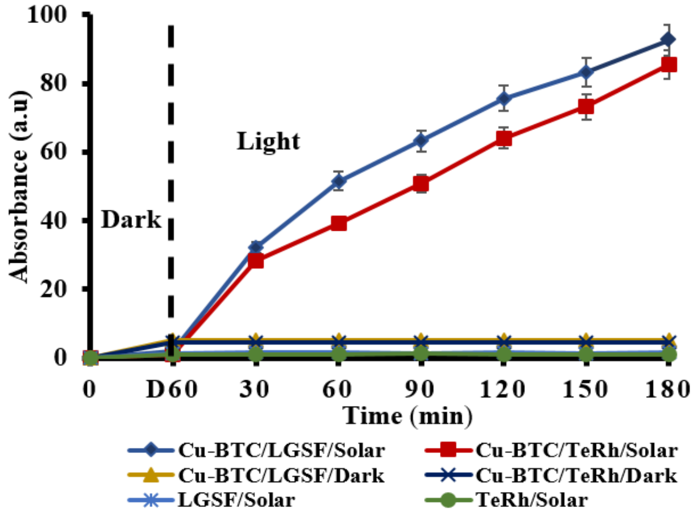


***Figure 7.*** *Photoactivity of* $[Cu_3(C_9H_3O_6)_2]._3H_2O\{18H_2O\}$ *(Optimum parameters: [Pollutant] = 0.20 g/L;* $[Cu_3(C_9H_3O_6)_2]._3H_2O\{18H_2O\}$ *Loading = 0.10 g/L; Solution pH = 6; Percentage error = 5%; Number of repeated experiment =3).*

This indicates $[Cu_3(C_9H_3O_6)_2]._3H_2O\{18H_2O\}$ is photoactive with efficient charge separation to generate radicals through an oxidation-reduction process during photolysis to mineralize LGSF and TeRh as indicated in Figure 8.

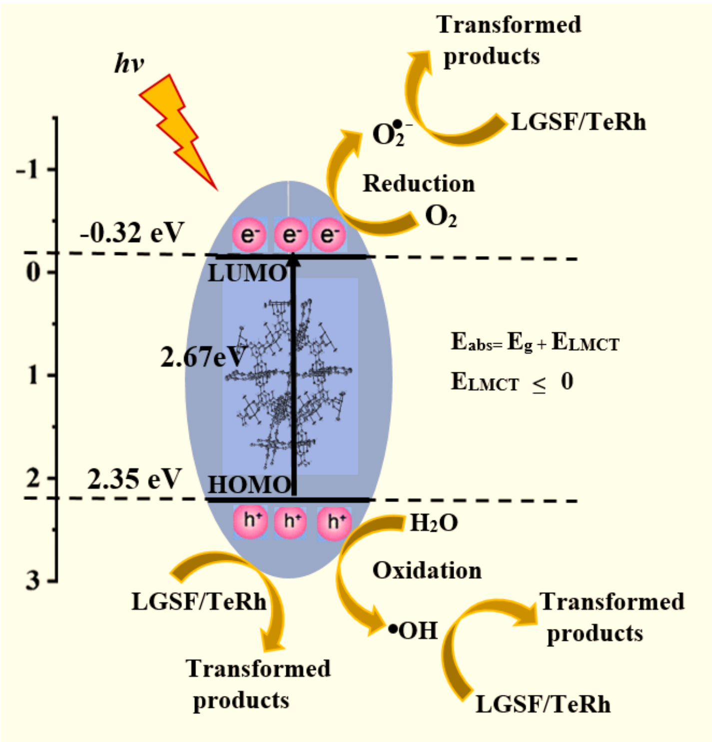


***Figure 8.*** *Band structure and Photocatalytic mechanism of* $[Cu_3(C_9H_3O_6)_2]._3H_2O\{18H_2O\}$*on LGSF and TeRh.*

A review of previously published literature on the photocatalytic degradation of organic dyes has shown that $[Cu_3(C_9H_3O_6)_2]._3H_2O\{18H_2O\}$ demonstrates comparable efficiency to what has been reported in Table 1. The results indicate that $[Cu_3(C_9H_3O_6)_2]._3H_2O\{18H_2O\}$ exhibits higher efficiency than HKUST-1 and MOF-199 in the mineralization of LGSF and TeRh pollutants (200 ppm), using a catalyst concentration of 100 mg/L (0.10 g/L). The efficiency of

$[Cu_3(C_9H_3O_6)_2]._3H_2O\{18H_2O\}$ in the mineralization of TeRh (Rhodamine B) can be compared to composites like $TiO_2$@HKUST-1, ZnO@HKUST-1, Ag/HKUST-1/ g-$C_3N_4$, and HKUST-1/PMS/Vis which require higher catalyst concentrations or lower pollutant concentrations. The unique properties of $[Cu_3(C_9H_3O_6)_2]._3H_2O\{18H_2O\}$, such as remarkable thermal stability, a large surface area, and substantial pore volume, contribute to its exceptional performance. The presence of $Cu^{2+}$ ions, which are redox active, enhances its photocatalytic effectiveness by participating in both oxidation and reduction reactions. Additionally, $[Cu_3(C_9H_3O_6)_2]._3H_2O\{18H_2O\}$maintains its structural integrity during the adsorption and desorption of water. Furthermore, the synthesis procedure for $[Cu_3(C_9H_3O_6)_2]._3H_2O\{18H_2O\}$is simple, making it a promising candidate for various photocatalytic applications.

*Table 1. Summary of reported photodegradation of dyes by Cu-BTC and Cu-BTC composites.*

| Cu-BTC, Cu-BTC based Photocatalyst | Pollutants | Pollutant concentration (ppm) | Catalyst loading (mg/L) | Irradiation time (min) | Efficiency (%) | Ref |
|---|---|---|---|---|---|---|
| HKUST-1 | Rhodamine B, Methylene blue | 10 | | 120 | 5.8, 53 | 46 |
| MOF-199 | Methylene blue | 5 | 40 | 300 | 88.96 | 45 |
| HKUST-1/PMS/Vis | Rhodamine B, Methylene blue | 10 | | 120 | 95 | 46 |
| GO/ ZIF-8/HKUST-1 | Congo red | 50 | 500 | 60 | 91 | 47 |
| CuO@HKUST− 1 | Methylene blue | 55 | 833.3 | 180 | 98 | 48 |
| Cu-$H_3$-btc–$Ag_2O$ | Orange G | 4.5 | 440 | 80 | 68.96 | 49 |
| $TiO_2$@HKUST-1 | Rhodamine B | | 300 | 120 | 95.20 | 50 |
| HKUST-1(Cu)/polymer | Acid Black | 15 | | 45 | 96 | 73 |
| ZnO@HKUST-1 | Rhodamine B | 20 | 320 | 45 | 97.4 | 51 |
| Ag/$Ag_3PO_4$/HKUST-1 | Biotrack 405 Blue caspase-3 dye (PBS) | | 1000 | 80 | 87 | 52 |
| Ag/HKUST-1/ g-$C_3N_4$ | Rhodamine B | 0.5 | 500 | 90 | 87.4 | 53 |
| $TiO_2$@HKUST-1 | Methylene blue | 20 | 500 | 60 | 91 | 54 |
| GO− CS@$Cu_3(btc)_2$ | Methylene blue | 10 | 500 | 60 | 98 | 55 |

The UV-visible absorption spectra of LGSF (640 nm) and TeRh (560 nm) are as shown in Figure 9. A gradual reduction of peaks at 30 min time intervals for 180 min was observed. This gradual reduction demonstrated that the pollutants were being removed from the sample solution.

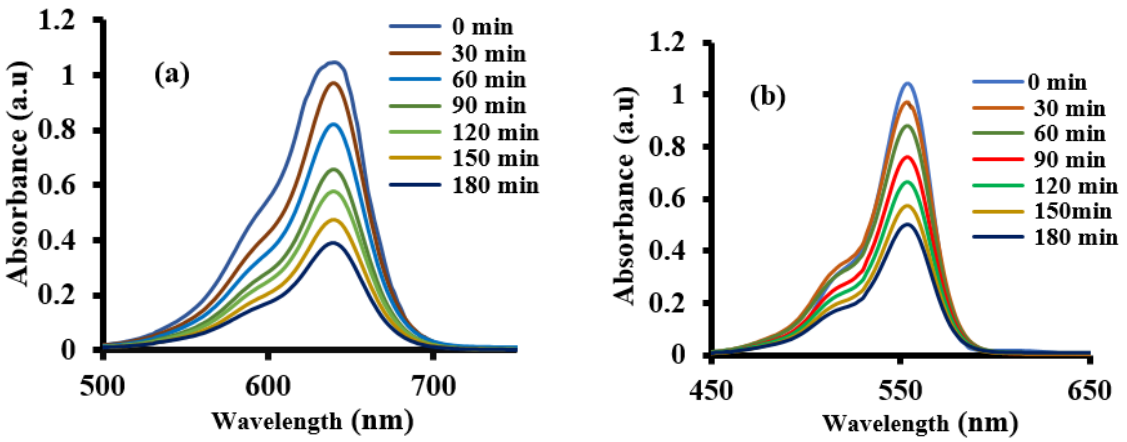


*Figure 9. Uv-visible absorption spectra of (a) Lissamine Green SF (LGSF) at 640 nm and (b) Tetraethylrhodamine (TeRh) at 560 nm under mineralization.*

The structures of the intermediates observed for the removal of LGSF and TeRh from water after gas chromatography-mass spectroscopy (GC-MS) analysis are shown in Table 2. LGSF (749.893 g/mol) was disintegrated into fragment compounds such as Phenol, 2, 2'-methylenebis [6-(1, 1-dimethylethyl)-4-methyl (m/z 340), 2, 6-di-tert-butyl-4-(2, 4, 6-trimethyl benzyl) phenol (m/z 338), 3-Phenyl-2-ethoxypropylphthalimide (m/z 309), 13-Tetradecenyl acetate (m/z 256), Phenol, 2, 4-bis(1, 1-dimethylethyl)-5-methyl (m/z 220) and Fumaric acid-ethyl-2-methylallyl ester (m/z 198). Fragment compounds observed for TeRh (479.02 g/mol) include 1, 2-benzene dicarboxylic acid, bis(2-ethylhexyl) ester (m/z 390), Dodecanoic acid, 4-nitrophenyl ester (m/z 321), 15-Hydroxypentadecanoic acid (m/z 258), 6-Hydroxy-4, 4, 5, 7-tetramethyl-2-chromanone (m/z 220) and 2, 5-Dimethyl-1, 5-hexadiene-3, 4-diol (m/z 142).

***Table 2.*** *Summary of Intermediates after 180 min Photoactivity on LGSF and TeRh.*

| | | | | | | |
|---|---|---|---|---|---|---|
| Lissamine green (LGSF) | Intermediates Percentage | | | | | |
| 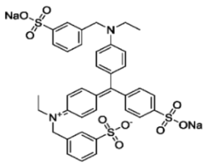 | 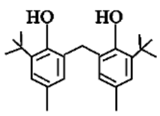 (m/z 340) | 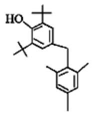 (m/z 338) | 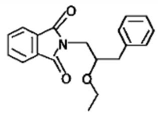 (m/z 309) | 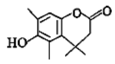 (m/z 220) | 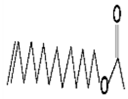 (m/z 256) | 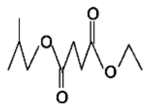 (m/z 198) |
| Time | | | | | | |
| 30 | (84%) | (96%) | (64%) | (49%) | -- | -- |
| 60 | (61%) | (62%) | (41%) | (46%) | (59%) | (13%) |
| 90 | (21%) | (52%) | (34%) | (93%) | (74%) | (21%) |
| 120 | (13%) | (23%) | (42%) | (71%) | (84%) | (62%) |
| 150 | (17%) | (11%) | -- | (67%) | (91%) | (89%) |
| 180 | -- | -- | -- | (31%) | (71%) | (97%) |
| Tetraethylrhodamine (TeRh) | Intermediates Percentage | | | | | |
| 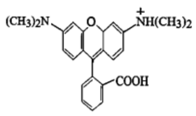 | 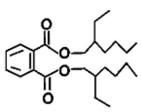 (m/z 390) | 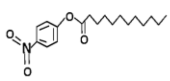 (m/z 321) | 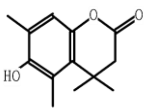 (m/z 220) | 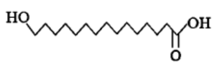 (m/z 258) | | 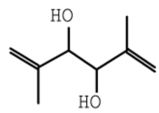 (m/z 142) |
| Time | | | | | | |
| 30 | (97%) | (54%) | (71%) | (13%) | | -- |
| 60 | (34%) | (66%) | (51%) | (37%) | | (21%) |
| 90 | (21%) | (42%) | (23%) | (42%) | | (26%) |
| 120 | (18%) | (35%) | -- | (78%) | | (73%) |
| 150 | (11%) | (19%) | (62%) | (74%) | | (82%) |
| 180 | -- | -- | (19%) | (93%) | | (97%) |

### 3.3. Reusability of $[Cu_3(C_9H_3O_6)_2]._3H_2O\{18H_2O\}$

That $[Cu_3(C_9H_3O_6)_2]._3H_2O\{18H_2O\}$ was observed in Figure 10 to be relatively stable with no considerable loss of activity over three cycles of the photocatalytic activity on Lissamine green SF (LGSF). This stability indicates its potential application for wastewater treatment.

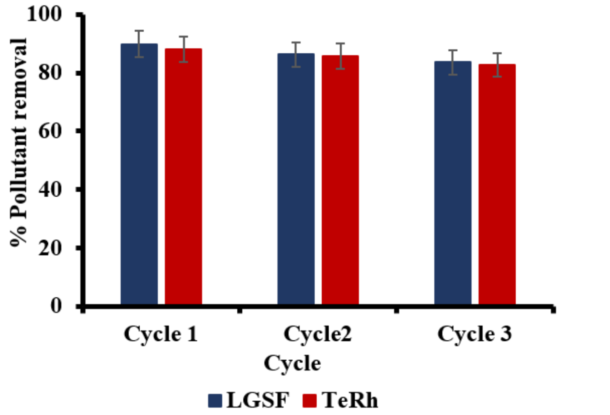


***Figure 10.*** *Cycle Test of $[Cu_3(C_9H_3O_6)_2]._3H_2O\{18H_2O\}$ on Pollutants (Percentage error = 5%).*

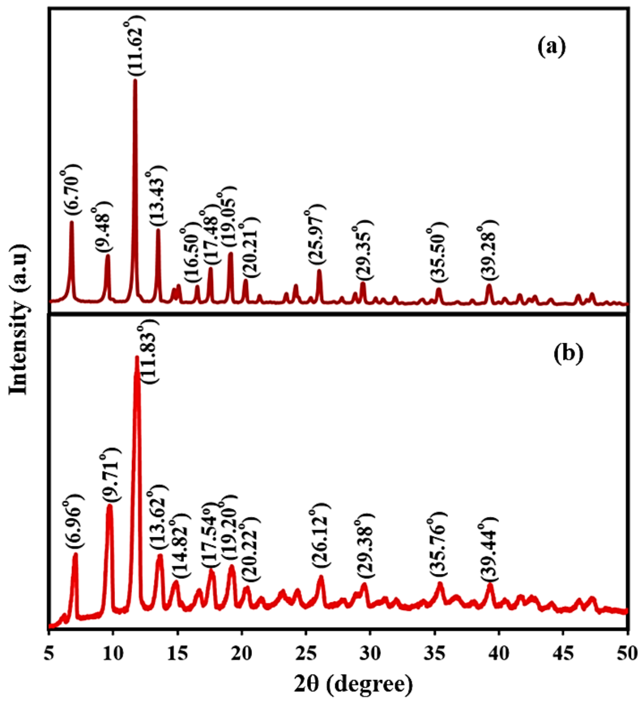


***Figure 11.*** *XRD of $[Cu_3(C_9H_3O_6)_2]._3H_2O\{18H_2O\}$ before (a) and after (b) Cycle photocatalytic transformation test.*

The X-ray diffraction (XRD) result of $[Cu_3(C_9H_3O_6)_2]._3H_2O\{18H_2O\}$before and after the cycle activity is shown in Figure 11. Similar diffraction peaks were observed after the cycle test confirming the stability of $[Cu_3(C_9H_3O_6)_2]._3H_2O\{18H_2O\}$. There was however a slight shift in diffraction peaks after the three-cycle activity which may have resulted in the slight decrease in photoactivity as observed in Figure 10.

SEM image of $[Cu_3(C_9H_3O_6)_2]._3H_2O\{18H_2O\}$ before and after the cycle activity is shown in Figure 12. Cubic crystal particles with trapezoid shapes similar to the morphology before the cycle was observed although closely packed. The closely packed morphology may be a result absorption of moisture.

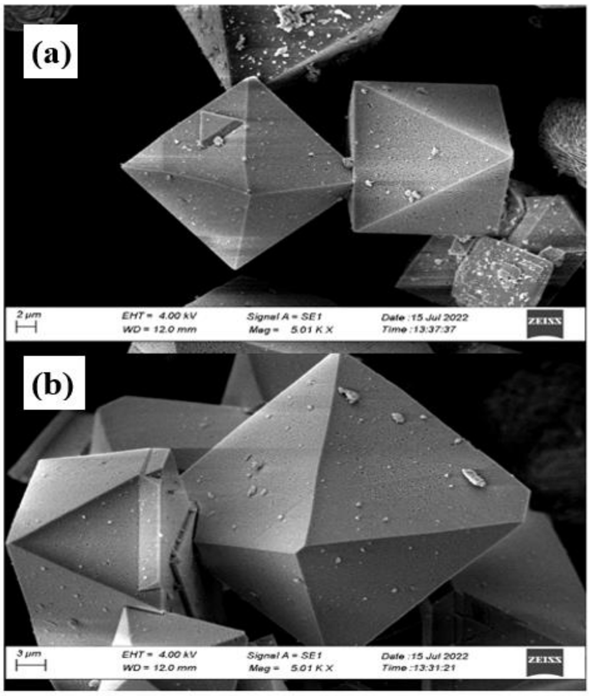


***Figure 12.*** *SEM of $[Cu_3(C_9H_3O_6)_2]._3H_2O\{18H_2O\}$ before (a) and after (b) Cycle photocatalytic transformation test.*

## 4. Conclusion

The key innovation of this work lies in the synthesis and characterization of the $[Cu_3(C_9H_3O_6)_2]._3H_2O\{18H_2O\}$ MOF and its application as a photocatalyst. The researchers hypothesized that the unique structural properties, high surface area, and optical properties of the MOF would contribute to its exceptional photocatalytic performance. The work aimed to explore the potential of $[Cu_3(C_9H_3O_6)_2]._3H_2O\{18H_2O\}$ in environmental remediation and sustainable chemistry. The newly synthesized $[Cu_3(C_9H_3O_6)_2]._3H_2O\{18H_2O\}$ MOF demonstrated remarkable potential as a photocatalyst for the mineralization of LGSF and TeRh under solar light irradiation. The study contributes to the field of photocatalysis by introducing a novel MOF material with high surface area, and unique optical properties. The work presents improvements in terms of photocatalytic activity and provides a foundation for future research aimed at optimizing the synthesis process, understanding the mechanism of action, and exploring practical applications.

## Abbreviations

| | |
|---|---|
| CB | Conduction Band |
| EDS | Energy Dispersive X-ray Spectroscopy |
| FTIR | Fourier Transform Infrared |
| HOMO | Highest Occupied Molecular Orbital |
| LMCT | Ligand-to-Metal Charge Transfer |
| LUMO | Lowest Unoccupied Molecular Orbital |
| MOF | Metal-organic Framework |
| SEM | Scanning Electron Microscope |
| TGA | Thermogravimetric |
| UV | Ultraviolet |
| VB | Valence Band |
| XRD | X-Ray Diffraction |

## Acknowledgements

The authors would like to thank the University of Cape Coast Chemistry Department laboratory for providing the necessary facilities and resources to carry out this study. The authors would like to acknowledge Dr Samuel Tetteh a Senior Lecturer at the Department of Chemistry, University of Cape Coast, Ghana and James Orton a Crystallographer at the National Crystallography Service, University of Southampton, UK, for their assistance in the deposition of the crystal structure of the synthesized metal-organic framework.

The crystal structure of $[Cu_3(C_9H_3O)_2].{}_3H_2O\{18H_2O\}$ determined has been deposited with a CCDC 2277633. https://doi.org/10.5517/ccdc.csd.cc2gg212.

## Author Contributions

**Aba Akebi Atta-Eyison:** Data curation, Formal Analysis, Investigation, Methodology, Resources, Writing – original draft

**Ruphino Zugle:** Conceptualization, Resources, Supervision, Writing – review & editing

## Conflicts of Interest

The authors declare no conflicts of interest.

## References

[1] A. A. Atta-Eyison, R. Zugle, Characterization of newly synthesized photoactive $[Cu_3(C_9H_3O_6)_2].{}_3H_2O\{18H_2O\}$ for the mineralization of Lissamine green SF (LGSF) and Tetraethylrhodamine (TeRh), Mendeley Data 1(2023). https://doi.org/10.17632/j4p6489t4s.1

[2] A. A Atta- Eyison, R. Zugle, Gas chromatography/mass spectrum (GC/MS) Results for the Mineralization of Lissamine Green SF and Tetraethylrhodamine.", Mendeley Data, V1(2024) https://doi.org/10.17632/mcnsrrbszw.1

[3] A. S Abdelmoaty, A. A. El-Beih, A. A. Hanna, Synthesis, characterization and antimicrobial activity of copper-metal organic framework (Cu-MOF) and its modification by melamine. Journal of Inorganic and Organometallic Polymers and Materials, 32(5), (2022), p. 1778-1785. https://doi.org/10.1007/s10904-021-02187-8

[4] E. C. Emenike, AGAdeniyi, PEOmuku, KCOkwu, KOIwuozor. Recent advances in nano-adsorbents for the sequestration of copper from water. Journal of Water Process Engineering. 1(47), (2022) p. 102-715. https://doi.org/10.1016/j.jwpe.2022.102715

[5] A. H. Shah, Z. U. Abideen, S. Maqsood, F. Rashid, R. Ullah, A. URehman, M. Dildar, M. Ahmad, K. Ullah, M. N. Rafi, F. Teng. Porous Cu-based metal organic framework (Cu-MOF) for highly selective adsorption of organic pollutants. Journal of Solid State Chemistry. Jun 1(322), (2023) p. 123-935. https://doi.org/10.1016/j.jssc.2023.123935

[6] H. W. Haso, A. A. Dubale, M. A. Chimdesa, M. Atlabachew. High performance copper based metal organic framework for removal of heavy metals from wastewater. Frontiers in Materials. Mar 8(9) (2022) p. 840-806. https://doi.org/10.3389/fmats.2022.840806

[7] A. Datta, M. Guleria, K. Kumar, J. Agarwal, R. Singh, V. Kaur, Copper (II) pseudoatrane appended heterobimetallic 2D‐MOF: A multi‐functional material with catalytic and sensing properties. Applied Organometallic Chemistry, 37(6) (2023) p. e7083. https://doi.org/10.1002/aoc.7083

[8] Y. Hua, X. Lv, Y. Cai, H. Liu, S. Li, Y. Wan, H. Wang, Highly selective and reproducible electroanalysis for histidine in blood with turn-on responses at a potential approaching zero using tetrahedral copper metal organic frameworks. Chemical Communications, 55(9), (2019) p. 1271-1274. https://doi.org/10.1039/C8CC09562K

[9] R, A. Peralta, M. T. Huxley, J. Albalad, C. J. Sumby, C. J. Doonan, Single-Crystal-to-Single-Crystal Transformations of Metal–Organic-Framework-Supported, Site-Isolated Trigonal-Planar Cu (I) Complexes with Labile Ligands. Inorganic Chemistry, 60(16), (2021) p. 11775-11783. https://doi.org/10.1021/acs.inorgchem.1c00849

[10] J. P. Vizuet, T. S. Howlett, A. L. Lewis, Z. D. Chroust, G. T. McCandless, K. J. Balkus Jr, Transition from a 1D coordination polymer to a mixed-linker layered MOF. Inorganic Chemistry, 58(8), (2019) p. 5031-5041. https://doi.org/10.1021/acs.inorgchem.9b00077

[11] D. Xu, Y. Yang, K. Le, G. Wang, A. Ouyang, B. Li, W. Liu, L. Wu, Z. Wang, J. Liu, F. Wang, Bifunctional Cu9S5/C octahedral composites for electromagnetic wave absorption and supercapacitor applications. Chemical Engineering Journal, (2021) p. 417. https://doi.org/10.1016/j.cej.2021.129350

[12] H. X. Zhang, Q. L. Hong, J. Li, F. Wang, X. Huang, S. Chen, S. Chen, W. Tu, D. Yu, R. Xu, T. Zhou, J. Zhang, Isolated square−planar copper centre in boron imidazolate nanocages for photocatalytic reduction of $CO_2$ to CO. Angewandte Chemie International Edition, 58(34), (2019) p. 11752-11756. https://doi.org/10.1002/anie.201905869

[13] J. Shen, X. Wang, L Zhang, Z. Yang, W. Yang, Z. Tian, J. Chen, T Tao. "Size-selective adsorption of methyl orange using a novel nano-composite by encapsulating HKUST-1 in hyper-crosslinked polystyrene networks." Journal of cleaner production, 184(2018) p. 949-958. https://doi.org/10.1016/j.jclepro.2018.03.015

[14] W. W. Lestari, M Adreane, C Purnawan, H Fansuri, N Widiastuti, S B Rahardjo. "Solvothermal and electrochemical synthetic method of HKUST-1 and its methane storage capacity." In IOP Conference Series: Materials Science and Engineering, 107(1) (2016) p. 012030. https://doi.org/10.1088/1757-899X/107/1/ 012030

[15] X. He, Y. Jin, M. Jia, M. Jia, H. Wang, M. Imran. MOF-derived carbon coated Cu 3 P with Ni doping as advanced supercapacitor electrode materials. Sustainable Energy & Fuels. 6(23) (2022) p. 5360-5370. https://doi.org/10.1039/D2SE01024K

[16] T. Baheri, Y. Yamini, M. Shamsayei, M. Tabibpour. Application of HKUST−1 metal−organic framework as coating for headspace solid−phase microextraction of some addictive drugs. Journal of Separation Science. 44(14) (2021) p. 281-423. https://doi.org/10.1002/jssc.202100070.

[17] M. Camats, D. Pla, M. Gómez. Copper nanocatalysts applied in coupling reactions: a mechanistic insight. Nanoscale. 13(45) (2021) p. 18817-18838. https://doi.org/10.1039/D1NR05894K

[18] M. P. Ravele, O. A. Oyewo, D. C. Onwudiwe. Controlled Synthesis of CuS and Cu9S5 and Their Application in the Photocatalytic Mineralization of Tetracycline. Catalysts. 11(2021) p. 899. https://doi.org/10.3390/catal11080899

[19] R. Kaur, A. Kaur, R. Kaur, S. Singh, M. S. Bhatti, A. Umar, S. Baskoutas, S. K. Kansal. Cu-BTC metal organic framework (MOF) derived Cu-doped $TiO_2$ nanoparticles and their use as visible light active photocatalyst for the decomposition of ofloxacin (OFX) antibiotic and antibacterial activity. Advanced Powder Technology. 32(5) (2021) p. 1350-1361. https://doi.org/10.1016/j.apt.2021.02.037

[20] Q. Wu, H. Ma, Y. Wang, J. Chen, J. Dai, X. Xu, X. Wu. Surface electron localization in Cu-MOF-bonded double-heterojunction Cu2O induces highly efficient photocatalytic $CO_2$ reduction. ACS Applied Materials & Interfaces. 14(48) (2022) p. 54328-54337. https://doi.org/10.1021/acsami.2c15278

[21] Z. Wang, Y. Xu, C. Wang, L. Yue, T. Liu, Q. Lan, X. Cao, B. Xing. Photocatalytic inactivation of harmful algae Microcystis aeruginosa and degradation of microcystin by g-$C_3N_4$/Cu-MOF nanocomposite under visible light. Separation and Purification Technology. 313(2023) p. 123515. https://doi.org/10. 1016/j.seppur.2023.123515

[22] X. Su, T. Xu, R. Ye, C. Guo, S. M. Wabaidur, D. L. Chen, S. Aftab, Y Zhong, Y. Hu. One-pot solvothermal synthesis of In-doped amino-functionalized UiO-66 Zr-MOFs with enhanced ligand-to-metal charge transfer for efficient visible-light-driven CO2 reduction. Journal of Colloid and Interface Science. 646(2023) p. 129-140. https://doi.org/10.1016/j.jcis.2023. 05.041

[23] S. Yang, W. Hu, J. Nyakuchena, C. Fiankor, C. Liu, E. D. Kinigstein, J. Zhang, X. Zhang, J. Huang. Unravelling a long-lived ligand-to-metal cluster charge transfer state in Ce–TCPP metal organic frameworks. Chemical Communications. 56(90) (2020) p. 13971-4. https://doi.org/10.1039/D0CC04116E

[24] Y. Zhao, J. Wang, R. Pei. Guest Molecules with Amino and Sulfhydryl Groups Enhance Photoluminescence by Reducing the Intermolecular Ligand-to-Metal Charge Transfer Process of Metal–Organic Frameworks. Applied Sciences. 12(22) (2022) p. 11467. https://doi.org/0.3390/app122211467

[25] Y. Zhao, J. Wang, W, Zhu, L. Liu R. Pei. The modulation effect of charge transfer on photoluminescence in metal–organic frameworks. Nanoscale, 13(8) (2021), 4505-4511. https://doi.org/10.1039/D0NR07834D

[26] K. An, H. Ren, D. Yang, Z. Zhao, Y. Gao, Y. Chen, J. Tan, W. Wang, Z. Jiang. Nitrogenase-inspired bimetallic metal organic frameworks for visible-light-driven nitrogen fixation. Applied Catalysis B: Environmental. 29(2021) p. 120167. https://doi.org/10.1016/j.apcatb.2021.120167

[27] P. P. Ferreira da Rosa, S. Miyazaki, H. Sakamoto, Y. Kitagawa, K. Miyata, T. Akama, M. Kobayashi, K. Fushimi, K. Onda, T. Taketsugu, Y. Hasegawa. Coordination geometrical effect on ligand-to-metal charge transfer-dependent energy transfer processes of luminescent Eu (III) complexes. The Journal of Physical Chemistry A. 125(1) (2021) p. 209-217. https://doi.org/10.1021/acs.jpca.0c09337

[28] H. Zhang, S. Si, G. Zhai, Y. Li, Y. Liu, H. Cheng, Z. Wang, P. Wang, Z. Zheng, Y Dai, T. X. Liu, B. Huang, B. Huang,. The long-distance charge transfer process in ferrocene-based MOFs with FeO6 clusters boosts photocatalytic CO2 chemical fixation. Applied Catalysis B: Environmental. (2023) p. 122909. https://doi.org/10.1016/j.apcatb.2023.122909

[29] S. B. Chanu, M. K. Raza, D. Musib, M. Pal, M. Pal, M. Roy. Potent Photochemotherapeutic Activity of Iron (III) Complexes on Visible Light-induced Ligand to Metal Charge Transfer. Chemistry Letters. 49(6) (2020) p. 724-727. https://doi.org/10.1246/cl.200139

[30] R. Das, S. S. Manna, B. Pathak, C. M. Nagaraja. Strategic design of Mg-centered porphyrin metal–organic framework for efficient visible light-promoted fixation of CO2 under ambient conditions: combined experimental and theoretical investigation. ACS applied materials & interfaces. 14(29) (2022) p. 33285-33296. https://doi.org/10.1021/acsami.2c07969

[31] R. Yin, Y. Chen, J. Hu, G. Lu, L. Zeng, W. Choi, M. Zhu. Complexes of Fe (III)-organic pollutants that directly activate Fenton-like processes under visible light. Applied Catalysis B: Environmental. 283(2021) p. 119663. https://doi.org/10.1016/j.apcatb. 2020.119663

[32] Q. Wang, Q. Gao, A. M. Al-Enizi, A. Nafady, S. Ma. Recent advances in MOF-based photocatalysis: environmental remediation under visible light. Inorganic Chemistry Frontiers. 7(2) (2020) p. 300-339. https://doi.org/ 10.1039/C9QI01120J

[33] S. Gautam, H. Agrawal, M. Thakur, A. Akbari, H. Sharda, R. Kaur, M. Amini. Metal oxides and metal-organic frameworks for the photocatalytic degradation: A review. Journal of Environmental Chemical Engineering. 8(3) (2020) p. 103726. https://doi.org/10.1016/j.jece.2020.103726

[34] M. T. Hang, Y. Cheng, Y. T. Wang, H. Li, M. Q. Zheng, M. Y. He, Q. Chen, Z. H. Zhang. Rational synthesis of isomorphic rare earth metal-organic framework materials for simultaneous adsorption and photocatalytic degradation of organic dyes in water. CrystEngComm. 24(3) (2022) p. 552-559. https://doi.org/10.1039/D1CE01411K

[35] C. Hou, X. Yuan, M. Niu, Y. Li, L. Wang, M. Zhang. In situ composite of Co-MOF on a Ti-based material for visible light multiphase catalysis: synthesis and the photocatalytic degradation mechanism. New Journal of Chemistry. 46(23) (2022) p. 11341-11349. https://doi.org/10.1039/D2NJ01294D

[36] X. Zhang, J. Wang, X. X. Dong, Y. K. Lv. Functionalized metal-organic frameworks for photocatalytic degradation of organic pollutants in environment. Chemosphere. 242(2020) p. 125144. https://doi.org/10.1016/j.chemosphere.2019.125144

[37] W. Huang, X. Wang, W. Zhang, S. Zhang, Y. Tian, Z. Chen, W. Fang, J. Ma Intraligand charge transfer boosts visible-light-driven generation of singlet oxygen by metal-organic frameworks. Applied Catalysis B: Environmental. 273(2020) p. 119087. https://doi.org/10.1016/j.apcatb.2020.119087

[38] G. Ramalingam, R. Pachaiappan, P. S. Kumar, S. Dharani, S. Rajendran, D. V. N. Vo, T. K. Hoang.. Hybrid metal organic frameworks as an Exotic material for the photocatalytic degradation of pollutants present in wastewater: a review. Chemosphere. 288(2022) p. 132448. https://doi.org/10.1016/j.chemosphere.2021.132448

[39] L. Wang, X. Li, B. Yang, K. Xiao, H. Duan, H. Zhao. The chemical stability of metal-organic frameworks in water treatments: Fundamentals, effect of water matrix and judging methods. Chemical Engineering Journal. 450(2022) p. 138215. https://doi.org/10.1016/j.cej.2022.138215

[40] W. Zhang, W. Huang, J. Jin, Y. Gan, S. Zhang. Oxygen-vacancy-mediated energy transfer for singlet oxygen generation by diketone-anchored MIL-125. Applied Catalysis B: Environmental. 292(2021) p. 120197. https://doi.org/10.1016/ j.apcatb.2021.120197

[41] M. Endashaw, T. Girma. Review on the removal of dyes by photodegradation using metal-organic frameworks under light irradiation. Chemistry and Materials Research, 12(1) (2020) p. 14-21.

[42] G. Su, T. Feng, Z. Huang, Y. Zheng, W. Zhang, G. Liu, W. Wang, H. Wei, L, Dang. MOF derived hollow CuO/ZnO nanocages for the efficient and rapid degradation of fluoroquinolones under natural sunlight. Chemical Engineering Journal. 436(2022) p. 135119. https://doi.org/10.1016/j.cej.2022.135119

[43] S. Li, S. Shan, S. Chen, H. Li, Z. Li, Y. Liang, J. Fei, L. Xie, J. Li. Photocatalytic degradation of hazardous organic pollutants in water by Fe-MOFs and their composites: A review. Journal of Environmental Chemical Engineering. 9(5) (2021) p. 105967. https://doi.org/10.1016/j.jece.2021.105967

[44] C. Yue, L. Chen, H. Zhang, J. Huang, H. Jiang, H. Li, S. Yang. Metal-organic framework-based materials: emerging high-efficiency catalysts for the heterogeneous photocatalytic degradation of pollutants in water. Environmental Science: Water Research & Technology. 9(3) (2023) p. 669-695. https://doi.org/10.1039/D2EW00784C

[45] D. Garg, H. Rekhi, H. Kaur, K. Singh, A. K. Malik. A novel method for the synthesis of MOF-199 for sensing and photocatalytic applications. Journal of Fluorescence. 32(3) (2022) p. 1171-1188. https://doi.org/10.1007/s10895-022-02902-9

[46] J. Zhang, C. Su, X. Xie, P. Liu, M. E. Huq. Enhanced visible light photocatalytic degradation of dyes in aqueous solution activated by HKUST-1: performance and mechanism. RSC advances. 10(61) (2020) p. 37028-37034. https://doi.org/10.1039/ D0RA05275B

[47] R. Ediati, L. L. Zulfa, I Maulidah, D. O. Sulistiono, H. Fansuri, A. Rosyidah, F. Martak, D. Hartanto, M. A. Abdullah, W. P. Utomo, E. N. Kusumawati. Addition of graphene oxide to ZIF-8/HKUST-1 composite for enhanced adsorptive and photocatalytic removal of congo red in wastewater. South African Journal of Chemical Engineering. 46(1) (2023) p. 132-142.

[48] M. Jin, X. Qian, J. Gao, J. Chen, D. K. Hensley, H. C. Ho, R. J. Percoco, C. M. Ritzi, Y. Yue. Solvent-free synthesis of CuO/HKUST-1 composite and its photocatalytic application. Inorganic Chemistry. 58(13) (2019) p. 8332-8338. https://doi.org/10.1021/acs.inorgchem.9b00362

[49] N. Tabatabaei, K. Dashtian, M. Ghaedi, M. M. Sabzehmeidani, E. Ameri. Novel visible light-driven Cu-based MOFs/Ag 2 O composite photocatalysts with enhanced photocatalytic activity toward the degradation of orange G: their photocatalytic mechanism and optimization study. New Journal of Chemistry. 42(12) (2018) p. 9720-9734. https://doi.org/10.1039/C7NJ03245E

[50] Y. Qiao, C. Sun, J. Jian, T. Zhou, X. Xue, J. Shi, G. Che, G. Liao. Efficient removal of organic pollution via photocatalytic degradation over a TiO2@ HKUST-1 yolk-shell nanoreactor. Journal of Molecular Liquids. 385(2023) p. 122383. https://doi.org/10.1016/j.molliq.2023.122383

[51] S. Roy, J. Darabdhara, M. Ahmaruzzaman. ZnO-based Cu metal–organic framework (MOF) nanocomposite for boosting and tuning the photocatalytic degradation performance. Environmental Science and Pollution Research. (42) (2023) p. 95673-95691. https://doi.org/10.1007/s11356-023-29105-4

[52] F. A. Sofi, K. Majid, O. Mehraj. The visible light driven copper based metal-organic-framework heterojunction: HKUST-1@ Ag-Ag3PO4 for plasmon enhanced visible light photocatalysis. Journal of Alloys and Compounds. 737(2018) p. 798-808. https://doi.org/10.1016/j.jallcom.2017.12.141

[53] Y. Qiao, Q. Han, D. Li, H. Li, B. Wei, G. Che, W. Jiang, W. Guan. Construction of novel Ag/HKUST-1/gC 3 N 4 towards enhanced photocatalytic activity for the degradation of pollutants under visible light. RSC advances. 9(71) (2019) p. 41591-41602. https://doi.org/ 10.1039/C9RA08489D

[54] M. Xiaobo, L. Xinyu, Z. Jie, H. Xiaoxian, Y. Weichun. Heterostructured TiO2@ HKUST-1 for the enhanced removal of methylene blue by integrated adsorption and photocatalytic degradation. Environmental Technology. 4(26) (2021) p. 4134-4414. https://doi.org/10.1080/09593330.2020.1745295

[55] M. S. Samuel, S Suman, E. Selvarajan, T. Mathimani, A. Pugazhendhi. Immobilization of Cu3(btc) 2 on graphene oxide-chitosan hybrid composite for the adsorption and photocatalytic degradation of methylene blue. Journal of Photochemistry and Photobiology B: Biology. 204(2020) p. 111809. https://doi.org/10.1016/j.jphotobiol.2020.111809

[56] S. Roy, J. Darabdhara, M. Ahmaruzzaman. Recent advances of Copper-BTC metal-organic frameworks for efficient degradation of organic dye-polluted wastewater: Synthesis, Mechanistic Insights and Future Outlook. Journal of Hazardous Materials Letters. 23(2023) p. 100094. https://doi.org/10.1016/j.hazl.2023.100094

[57] L. Yang, G. L. Ruess, M. A. Carreon, Cu, Al and Ga based metal organic framework catalysts for the decarboxylation of oleic acid. Catalysis Science & Technology, 5(5), (2015) p. 2777-2782. https://doi.org/10.1039/C4CY01609B

[58] A. K. Kar, R. Srivastava, An efficient and sustainable catalytic reduction of carbon–carbon multiple bonds, aldehydes, and ketones using a Cu nanoparticle decorated metal organic framework. New Journal of Chemistry, 42(12), (2018) p. 9557-9567. https://doi.org/10.1039/C8NJ01704B

[59] R. Nivetha, A. Sajeev, A. M Paul, K. Gothandapani, S. Gnanasekar, P. Bhardwaj, G. Jacob, R. Sellappan, V. Raghavan, K. Chandar, S. Pitchaimuthu, S. K Jeong, A. N. Grace, Cu based Metal Organic Framework (Cu-MOF) for electrocatalytic hydrogen evolution reaction. Materials Research Express, 7(11), (2020) p. 114001. https://doi.org/10.1088/2053-1591/abb056

[60] C. Ardila-Suárez, A. M. Díaz-Lasprilla, L. A. Díaz-Vaca, P. B. Balbuena, V. G. Baldovino-Medrano, G. E. Ramírez-Caballero, Synthesis, characterization, and post-synthetic modification of a micro/ mesoporous zirconium–tricarboxylate metal–organic framework: Towards the addition of acid active sites. CrystEngComm, 21(19), (2019) p. 3014-3030. https://doi.org/10.1039/C9CE00218A

[61] X. Guo, C. Lin, M. Zhang, X. Duan, X. Dong, D. Sun, T. You, 2D/3D Copper-Based Metal-Organic Frameworks for Electrochemical Detection of Hydrogen Peroxide. Frontiers in Chemistry, 9, (2021) p. 743637. https://doi.org/10.3389/fchem.2021.743637

[62] J. Al Cheikh, A. Villagra, A. Ranjbari, A. Pradon, M. Antuch, D. Dragoe, L. Assaud, Engineering a cobalt clathrochelate/ glassy carbon interface for the hydrogen evolution reaction. Applied Catalysis B: Environmental, 250, (2019) p. 292-300. https://doi.org/10.1016/j.apcatb.2019.03.036

[63] A. B. D. Nandiyanto, R. Oktiani, R. Ragadhita, How to read and interpret FTIR spectroscope of organic material. Indonesian Journal of Science and Technology, 4(1), (2019) p. 97-118.

[64] S. Nzikayel, I. J. Akpan, E. C. Adams, Synthesis, ftir and electronic spectra studies of metal (ii) complexes of pyrazine-2-carboxylic acid derivative. Medicinal Chemistry, 7(11), (2017) p. 2161-444. https://doi.org/10.4172/2161-0444.1000475

[65] G. M. Sheldrick, Crystal structure refinement with ShelXL, Acta Cryst. C71(2015a) p. 3-8. https://doi.org/10.1107/S2053229614024218

[66] G. M. Sheldrick, ShelXT-Integrated space-group and crystal-structure determination, Acta Cryst. A71(2015b) p. 3-8. https://doi.org/10.1107/S2053273314026370

[67] A. S. Mukasyan, DTA/TGA-based methods. In Concise Encyclopedia of Self-Propagating High-Temperature Synthesis. Elsevier. (2017) p. 93-95. https://doi.org/10.1016/B978-0-12-804173-4.00040-5

[68] F. Yakuphanoglu, Thermal analysis methods used in solid state physics and chemistry to obtain kinetics and thermodynamics parameters of solid materials by TGA, DTA and DSC analyses. Journal of Materials and Electronic Devices, 1(1), (2019) p. 17-23.

[69] A. A. Scharnberg, A. C. De Loreto, A. K. Alves. Optical and structural characterization of Bi2FexNbO7 nanoparticles for environmental applications. Emerging Science Journal. 4(1) (2020) p. 11-17. https://doi.org/10.28991/esj-2020-01205

[70] H. Siddiqui, M. S. Qureshi, F. Z. Haque. pH-dependent single-step rapid synthesis of CuO nanoparticles and their optical behavior. Optics and Spectroscopy. 123(2017) p. 903-912. https://doi.org/10.1134/S0030400X17120013

[71] W. Brostow, G. Granowski, N. Hnatchuk, J. Sharp, J. B. White. Thermoelectric phenomena. J. Mater. Educ. 36(5-6) (2014) p. 175-186.

[72] F. Roccaforte, G. Brezeanu, P. M. Gammon, F. Giannazzo, S. Rascunà, M. Saggio, M. Schottky. contacts to silicon carbide: Physics, technology and applications. Advancing Silicon Carbide Electronics Technology, I: Metal Contacts to Silicon Carbide: Physics, Technology, Applications. (2018) p. 9781945291852-3. https://doi.org/10.21741/9781945291 852

[73] C. Brahmi, M. Benltifa, C. Vaulot, L. Michelin, F. Dumur, F. Millange, M. Frigoli, Airoudj A, Morlet-Savary F, Bousselmi L, Lalevée J. New hybrid MOF/polymer composites for the photodegradation of organic dyes. European Polymer Journal. 154(2021) p. 110560. https://doi.org/10.1016/j.eurpolymj.2021.110560

## Research Fields

**Aba Akebi Atta-Eyison:** Chemistry, Coordination chemistry, Catalysis, Analytical Chemistry, Organic Chemistry, Environmental Chemistry

**Ruphino Zugle:** Chemistry, Analytical Chemistry, Organic Chemistry, Coordination Chemistry, Catalysis, Environmental Chemistry